CALPHAD: Computer Coupling of Phase Diagrams and Thermochemistry 54 (2016) 82–96

Contents lists available at ScienceDirect

CALPHAD: Computer Coupling of Phase Diagrams and Thermochemistry

journal homepage: www.elsevier.com/locate/calphad

Inherently consistent temperature function for interaction parameters demonstrated for the Mg–Si assessment

Song-Mao Liang, Peisheng Wang, Rainer Schmid-Fetzer *

Institute of Metallurgy, Clausthal University of Technology, Robert-Koch-Str. 42, D-38678 Clausthal-Zellerfeld, Germany

ARTICLE INFO

Article history:
Received 11 March 2016
Received in revised form
13 June 2016
Accepted 14 June 2016

Keywords:
Excess Gibbs energy
Temperature dependence
Interaction parameters
Mg–Si system

ABSTRACT

A new inherently consistent temperature function for interaction parameters, L, is proposed. It is designed for the unconstrained application of any optimization software, such as PanOptimizer or PARROT, to avoid artifacts, for example inverted liquid miscibility gaps or re-stabilization of liquid well below solidus. Without introducing additional system-dependent adjustable parameters, the new function automatically excludes both the exaggerated negative values of L at low temperature and the exaggerated positive values of L at high temperature. The viability of the new function is demonstrated by a complete Calphad re-assessment of the Mg–Si system, which is the prime example of the most challenging systems pertinent to both artifacts. For the first time the calculated Mg–Si phase diagram from 0 K to very high temperature is presented. The new assessment also includes the quantitative solidus data of (Si) and other previously not considered original experimental data.

1. Introduction

The temperature dependence of interaction parameters in non-ideal solution phases is still a controversial issue. From a practical point of view, linear temperature dependence is usually assumed for the interaction parameters of solution phases as a reasonable approximation. However, this may result in artifacts, the inverse miscibility gap of a liquid phase being the most prominent example.

To be more specific, this study will focus on the most common description of the Gibbs energy for the liquid phase of a binary system in the approximation of the substitutional solution model with a Redlich–Kister polynomial [1] as follows:

$$G^{\mathrm{Liquid}} = x_1 \cdot G_1^{0,\mathrm{Liquid}} + x_2 \cdot G_2^{0,\mathrm{Liquid}} + \mathrm{R}\cdot T\cdot\left(x_1\cdot \ln x_1 + x_2 \cdot \ln x_2\right) + x_1 \cdot x_2\left[L_{1,2}^{0,\mathrm{Liquid}} + L_{1,2}^{1,\mathrm{Liquid}}(x_1 - x_2) + L_{1,2}^{2,\mathrm{Liquid}}(x_1 - x_2)^2 + \ldots\right] \quad (1)$$

where x_1, x_2 represent the molar fractions of components $(i)=1,2$, respectively. T is the absolute temperature and R is the gas constant ($R=8.3145\ \mathrm{J\ mol^{-1}\ K^{-1}}$). The reference state for the pure liquid components, $G_i^{0,\mathrm{Liquid}}(T)$, will be detailed later in the application to Mg–Si. The parameters $L_{1,2}^{\nu,Liquid}$ represent the interaction of order ν between elements (1) and (2) in the liquid phase in the Redlich–Kister approximation. A linear temperature dependence is usually used for the interaction parameter $L_{1,2}^{\nu,Liquid}$ with constant values of the adjustable parameters A^{ν} and B^{ν}:

$$L_{1,2}^{\nu,Liquid} = A^{\nu} + B^{\nu}\cdot T \quad (2)$$

However, it was revealed in the study of Chen et al. [2] that for liquid phases the distracting artifact of an inverted miscibility gap may occur at high temperature. This was quite often overlooked in previously published assessments. The problem is usually related to a bad choice of the entropy related parameter, B»0, as pointed out by Kaptay [3]. To simplify the notation we will omit the sub- and superscripts and focus on one representative parameter, L, standing for $L_{1,2}^{\nu,Liquid}$. In case of Eq. (2) we have $L=\mathrm{A}+\mathrm{B}\cdot T$.

One way to solve the inverted miscibility gap problem is by imposing thermodynamic constraints ($\partial^2 G^{\varphi}/\partial x^2>0$) as decribed by Lukas et al. [4]. However, this additional constraint will make it harder to fit the actual experimental data in the thermodynamic assessment. Another approach was suggested by Kaptay [3] with an exponential function for L:

$$L = h\cdot\exp(-T/\tau) \quad (3)$$

Here h and τ are the two adjustable parameters with $\tau > 0$. Indeed, since $L\to 0$ for $T\to\infty$, the inverted miscibility gap does not occur. However, as shown later by Schmid-Fetzer et al. [5], a simple choice of the parameters h and τ may produce another distracting artifact, the re-stabilization of the liquid phase at low temperature, as demonstrated very roughly for the Mg–Si system [5]. Even though no full Calphad assessment was performed [5], this rough demonstration showed that the parameters h and τ must be very carefully selected, which impedes an unconstrained parameter

* Corresponding author.
E-mail address: schmid-fetzer@tu-clausthal.de (R. Schmid-Fetzer).

http://dx.doi.org/10.1016/j.calphad.2016.06.003
0364-5916/

optimization. It is possible to find such parameters as shown by Yuan et al. [6] for the Mg–Si system, but the problem for unconstrained parameter optimization with Eq. (3) persists.

Subsequently, Kaptay [7] suggested a combination of the linear and exponential temperature functions in an attempt to avoid both artifacts:

$$L = (h - s{\cdot}T)\exp(-T/\tau) \quad (\text{with } \tau > 0) \tag{4}$$

Here three adjustable parameters, h, s, and τ, are used. No example of complete Calphad optimization for any real system was given. It was admitted, though, that observance of a delicate balance among the three parameters (h, s, τ) may be required to exclude any low temperature artifact [7]. This function for L is, thus, not inherently consistent.

Guidelines for an inherently consistent function were already given in [5]. The function should tend to zero at high temperature but without an excessive increase at low temperature. A multiplier function was suggested, such as

$$L = (a + b{\cdot}T){\cdot}\mathrm{f}(T) \tag{5}$$

In general, f(T) should have a "smooth" S-shape behavior, with an analytical derivative and also be computationally efficient. That rules out the error function, for example; beyond these general guidelines no function f(T) was specified [5].

In the present work such a new temperature function for L is proposed which is inherently consistent. That is important for the unconstrained application of any optimization software, such as PanOptimizer or PARROT. Without introducing additional system-dependent adjustable parameters, the new function excludes both the exaggerated negative values of L at low T and the exaggerated positive values of L at high T. The viability of the new function is demonstrated by a complete Calphad re-assessment of the Mg–Si system, which is the prime example of the most challenging systems pertinent to both artifacts.

2. General features of the new function for *L*-parameters

The first guideline for Eq. (5) was that the function should tend to zero at high temperature. This follows the claim made by Lupis and Elliot in 1966 [8] "Quite generally an increase in the temperature tends to bring a system closer to ideality". Their correlation between excess entropy and enthalpy functions [8] was analyzed in more detail by Kaptay [3,7,9] based on reported thermodynamic properties of a large number of real solution phases. The rule boils down to the condition that the excess Gibbs energy of a solution phase, G^{exc}, given for example by the second line of Eq. (1), must tend towards zero at infinite temperature. All other excess properties will then also tend to zero together with the temperature derivatives of G^{exc}. The same holds true for all the L-parameters, defining the temperature dependence of G^{exc}. The second guideline for Eq. (5) was to exclude excessive increase at low temperature. Following these guidelines the new function for L-parameters, briefly denoted as *LET*, is defined as follows

$$L = (a + b{\cdot}T){\cdot}E(T) \tag{6}$$

where the term $E(T)$ stands for

$$E(T) = \exp\left[-\left(\frac{T - T_1}{\sqrt{2}{\cdot}T_2}\right)^2\right] \tag{7a}$$

Here T_1 and T_2 are two constant temperatures, selected by reviewing the range of melting points for most of the important elements. The design of $E(T)$ is based on the simple function $\exp(-x^2)$ which has a maximum at $x=0$ and a point of inflection at $x=1/\sqrt{2}$. The $E(T)$ function is shifted to show its maximum at T_1 and scaled to get the point of inflection at T_1+T_2. This is given in more detail by the first and second derivative of $E(T)$:

$$E'(T) = -\frac{T - T_1}{T_2^2}{\cdot}E(T) \tag{7b}$$

$$E''(T) = \frac{(T - T_1)^2 - T_2^2}{T_2^4}{\cdot}E(T) \tag{7c}$$

Therefore, at $T = T_1$ we have $E'(T) = 0$ and $E(T)$ reaches the maximum value of 1. When $T = T_1 + T_2$ we have $E''(T) = 0$, which corresponds to the inflection point of E(T).

Fixed values of 500 K and 2000 K for T_1 and T_2, respectively, are generally suggested. Thus, the term $E(T)$ is described by:

$$E(T) = \exp\left[-\left(\frac{T - 500\mathrm{K}}{\sqrt{2}{\cdot}2000\mathrm{K}}\right)^2\right] \tag{7d}$$

As alternative procedure one might also use simply the melting points of the pure elements forming the binary system to be assessed. However, that may lead to problems in ternary or higher order systems, when assigning intermediate melting temperatures. An alternative choice of $T_1=0$ and $T_2=2500$ K will also be shown below to discuss the impact of this choice on excess properties. The most important point is that T_1 and T_2 are made to be fixed values and not adjustable parameters, independent of any interaction in the binary system. Therefore, the new function *LET* has only two adjustable parameters, a and b in Eq. (6).

Fig. 1 shows the temperature dependence of the basic function $E(T)$ as proposed from Eq. (7d), temporarily named $E(500, 2000;T)$, together with the alternative choice for discussion, $E(0, 2500;T)$. The first function has its maximum at 500 K, the latter at 0 K. Both have their point of inflection at 2500 K at the same value of $E=0.61$. A key feature is that $E(T)$ does not vary too much in a temperature range around 1500 K which is considered most relevant for practical applications. This feature is more pronounced for the first function, Eq. (7d), which is the reason for accepting it in this work. At higher temperatures both functions approach zero, as intended.

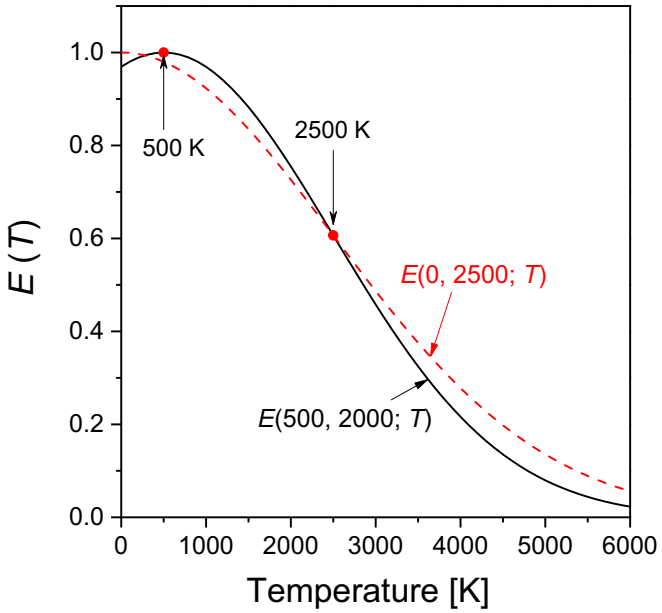

Fig. 1. The basic $E(T)$ function plotted versus temperature in two options. Solid line: $E(500, 2000; T)$ with $T_1=500$ K; $T_2=2000$ K, accepted in this work. Dashed line: $E(0, 2500; T)$ with $T_1=0$ K; $T_2=2500$ K, alternative for discussion.

In order to compare the new *LET* function in Eq. (6) to the classical linear expression in Eq. (2) let us assume a hypothetical A–B system with the parameters $L^0_{A,B}$ for the liquid phase

$$L^0_{A,B} = -120,000 + 50 \cdot T \tag{8}$$

These arbitrarily selected parameters may be suitable to describe experimental data around 1500 K in an assumed temperature range of 500 to 2500 K. At higher temperature, however, this setting produces an artifact. As shown in Fig. 2(a) above the critical temperature, $T_{c,min} = a/(-b+2 \cdot R) = 3595$ K, an inverted miscibility gap emerges in the liquid phase. Instead of $L^0_{A,B}$ the excess Gibbs energy of this simple regular solution phase is plotted in Fig. 2 (a) at mid-composition of 50 at% A, $G^{exc} = 0.25\, L^0_{A,B}$.

By fitting the two parameters a and b of the *LET* function in Eq. (6) to the value and slope at 1500 K given by the linear function $L^0_{A,B} = -120,000 + 50 \cdot T$ the corresponding alternative *LET* functions denoted as *LET* and *LET*-2 in Fig. (2) are obtained:

$$LET: L^0_{A,B} = (-116,856 + 43.910 * T) * E(500, 2000; T) \tag{9a}$$

$$LET-2: \quad L^0_{A,B} = (-124,271 + 46.931 * T) * E(0, 2500; T) \tag{9b}$$

It is noted that for the latter choice with $T_1 = 0$ and $T_2 = 2500$ K the *LET* function does not reduce to the combination of the linear and exponential temperature functions in Eq. (4) because *LET* still carries the $\exp(-T^2)$ term as opposed to the $\exp(-T)$ term in Eq. (4). The G^{exc} curves from these *LET* functions almost coincide with the linear function in the temperature range of about 500–2000 K in Fig. 2. At higher temperature the decaying part $E(T)$ in the function becomes dominant and the *LET* functions attain only small positive values before approaching zero, as intended. Below about 500 K the values of the *LET* function do not change dramatically, staying close to the linear extrapolation. Excessive values are inherently excluded because the basic $E(T)$ function gives values in the order of unity in the low temperature range.

Also shown for comparison in Fig. 2 is the exponential function, see Eq. (3), since it also employs two parameters only. These are also fitted to the value and slope at 1500 K given by the linear function, resulting in

$$L^0_{A,B} = -238,252 \cdot \exp(-T/900\ \mathrm{K}) \tag{10}$$

At high temperature this function also approaches zero. In the medium temperature range the agreement with the linear data is observed in a narrow range only due to the strong curvature. The

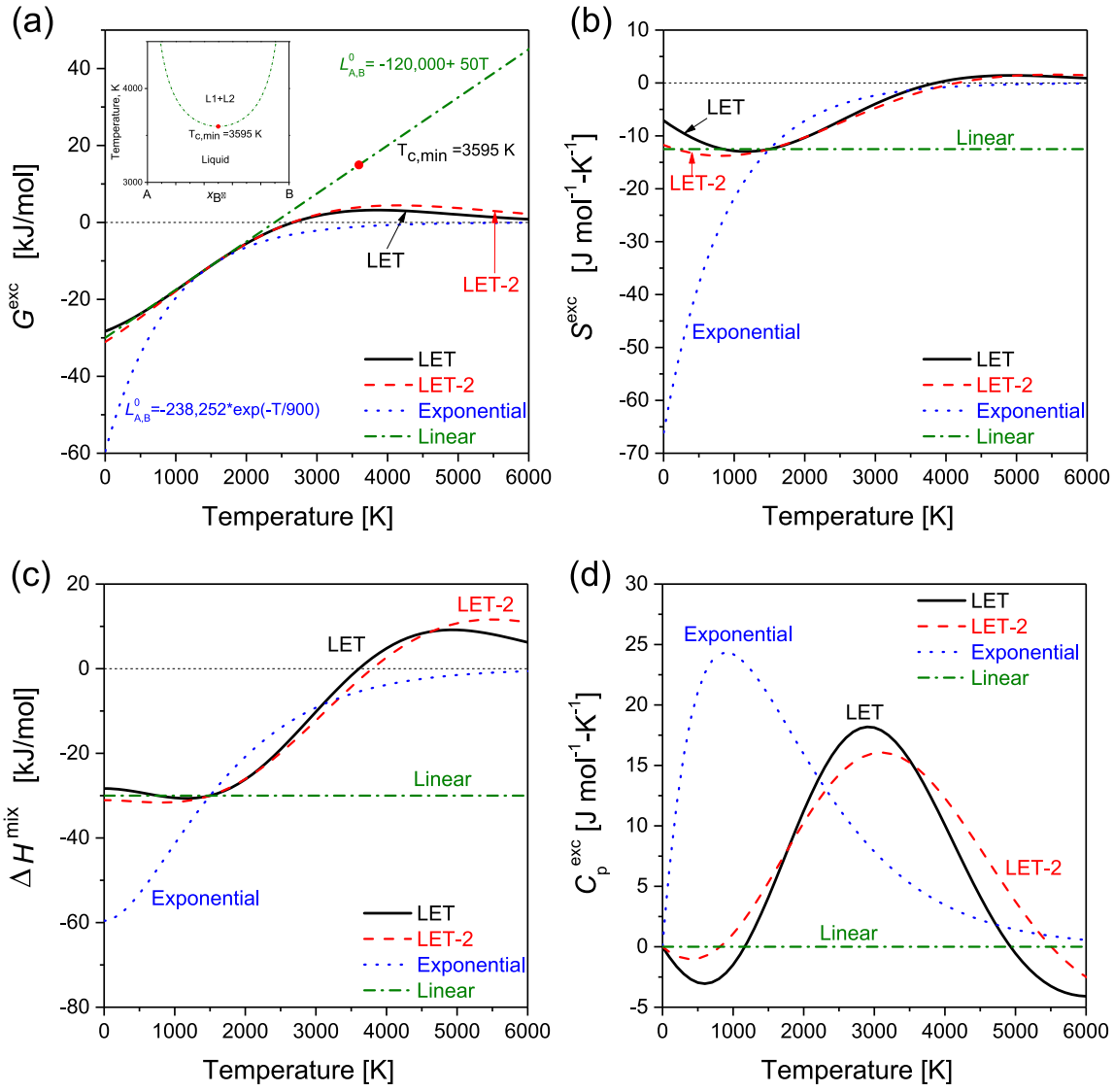

Fig. 2. Excess properties of the regular solution phase at 50 at% A in A–B system. (a) Excess Gibbs energy; (b) excess entropy; (c) enthalpy of mixing; (d) excess heat capacity. The four hypothetical regular solution parameters are given in the text: LET Eq. (9a), LET-2 Eq. (9b), Exponential Eq. (10), and Linear Eq. (8).

most distracting feature is the excessive negative value in the low temperature range. The extrapolated value at 0 K is essentially twice the value of the *LET* or linear functions. That is exactly the feature requiring distracting constraints on optimizing the parameters (h and τ) to avoid the artifact of liquid re-stabilization at low temperature. This function type is, just like the linear function, not inherently consistent.

It is noted that the slope of G^{exc} from both *LET* functions at $T = 0$ K is not zero. This is not considered a contradiction to thermodynamic laws because the negative value of the slope relates not to the entropy but to the excess entropy. The excess entropy, S^{exc}, shown in Fig. 2(b) is calculated from the negative slope of the four curves in Fig. 2(a). The shallow minimum in the curves at 800 K (*LET-2*) or 1200 K (*LET*) has no physical meaning. The intention of the heuristic *LET* functions is accomplished by avoiding excessively large values at low temperatures as shown by comparison to the exponential function.

The enthalpy of mixing is shown in Fig. 2(c), all four curves intersect exactly at 1500 K and $\Delta H^{mix} = -30$ kJ/mol, as designed. It is noted that in most alloys systems for which experimental data for the temperature dependence of ΔH^{mix} of the liquid phase are available this temperature dependence is usually fairly small unless the liquid shows strong short-range order. To resemble this general experience with a simple analytical function was a key intention in developing the *LET* function. This is comparably well accomplished as demonstrated in Fig. 2(c). The values of ΔH^{mix} are approximately constant in a temperature range up to about 2000 K. As opposed to that, the exponential function shows a very strong temperature dependence in that range. At very high temperature all curves – except the linear one – approach zero values, as intended. The maxima of ΔH^{mix} in the *LET* curves around 5000 K are considered irrelevant because of the high temperatures; they are due to the competition of the $(a+b\cdot T)$ term (with b»0) and the $E(T)$ term in Eq. (6). These maxima might be avoided by using, instead of *LET*, a "magic function" that is linear from 0 to 2000 K, beyond that veers off to zero at infinite temperature without changing sign, with continuous first and second derivative. We did not find an analytical function doing that.

The calculated slopes of ΔH^{mix} provide the curves for the excess heat capacity, C_p^{exc}, in Fig. 2(d). Relatively small values are given by the *LET* curves as opposed to the exponential function in the range up to 1500 K. The high-temperature maximum of the *LET* curve at 2900 K with $C_p^{exc} = 18$ J mol^{-1} K^{-1} is in principle unavoidable. Even if using the "magic function" from the previous paragraph a single high-temperature maximum of C_p^{exc} must exist if we demand ΔH^{mix} to be constant (e.g. -30 kJ mol^{-1}) at lower temperature and approaching zero (ideal behavior) at infinite temperature. All four curves of C_p^{exc} approach zero values at very high temperature.

The general experimental experience of a small temperature dependence of ΔH^{mix} (or the bond energy in a regular solution model) relates to small values of C_p^{exc}. From that point of view the linear equation would be "best" with $C_p^{exc} = 0$. However, this choice cannot avoid the high temperature artifact shown in Fig. 2(a) and it is inconsistent with the approach to ideal solution behavior at very high temperature. By reviewing Fig. 2(a)–(d) it is also obvious that the proposed *LET* function depends only little on the alternative choice of the values of T_1 and T_2. This supports the present proposal to use these as fixed values and not adjustable parameters. More sophisticated solution models, such as the modified quasi-chemical model or the associated solution model and the impact on the excess properties of the liquid will be discussed later for the case of the real systems Mg–Si and Mg–Sn. It will also be shown in these examples that in real systems with more than one L-parameter of different signs more complex excess properties are generated.

In summary, the proposed *LET* function combines several advantages. It is similar to a linear relation in a wide temperature range, usually accessible to experimental data, and avoids excessive values of the interaction parameter at very high and very low temperatures. Only two adjustable parameters are used in this relatively simple analytical function. All of these features are intrinsic by design and, thus, the *LET* function is inherently consistent, no matter what values are chosen for the adjustable parameters a and b in Eq. (6). The term inherently consistent is not used in a physical sense but for the practical, unconstrained optimization of this interaction parameter in a Calphad assessment.

3. Experimental data basis of the Mg–Si system

The theoretical advantages of the new *LET* function shall be validated by a complete Calphad re-optimization of the Mg–Si system, which is the prime example of the most challenging systems pertinent to both artifacts, at very high and very low temperatures.

Extensive investigations have been carried out on the Mg–Si binary system. Nayeb-Hashemi and Clark [10], which is the same as [11], reviewed all experimental results before 1984. The experimental results have also been collected and reviewed by Yuan et al. [6] and Schick et al. [12] for their Calphad assessments. Since then, no more new experimental data on Mg–Si system have been published. In this work, detailed discussions and review of experimental methods and data will not be repeated, but we have collected all experimental data from the original papers, and evaluated the data carefully. Therefore, a number of experimental data shown here differ somewhat from those shown in previous Calphad assessments [6,12,13] (detailed extracted original data see the appendix excel file). Here we only report our treatment on the experimental data for thermodynamic modeling.

For the phase equilibria, the experimental data from [12,14–18] are accepted for optimization. Other experimental data [19–22] will be presented for comparison. For the liquidus and invariant reactions data, we put more weight on [14] over other experimental data. Their dedicated experiments will be further discussed later in the results and discussion section. The solubility of Si in (Mg) is optimized based on the experimental data in [15], which is close to the estimation in [16]. The solubility of the Mg in (Si) is thermodynamically assessed for the first time based on the experimental data from [17].

The activities of Mg in the liquid phase data have been measured by vapor pressure [23] and electromotive force (EMF) measurement [24,25]. The EMF measurements agree with each other [24,25], but are lower than the activity values obtained from the vapor pressure measurement [23]. As pointed out by previous researchers [6,11,18], it would be difficult to construct a reversible electromotive force cell for Mg–Si system, thus the vapor pressure data could be more reliable. In this work, the activity data from [23] are accepted for optimization, while the data from [24,25] are only used for comparison. Actually, we have also tried to only use the activity of [24,25] for optimization. We found that it is difficult to fit these activity data well together with a reasonable agreement of the phase equilibria data. We did not accept the revised values reported in [18], because only the data in [23] were original data, and the revised values in [18] were actually calculated values based on their determined phase diagram to adjust the activity data obtained from vapor pressure. No direct measured experimental data on the enthalpy of mixing of the liquid phase is available in the literature, except the low temperature calorimetric measurements in Mg-rich alloys [26]. Several sets of enthalpy of mixing values have been published derived from vapor pressure [18,23], EMF measurements [24,25] or calculated from low

temperature calorimetric measurements [26]. We have to emphasize that all these derived data can not be used for optimization. A clear example is that based on the same sets of original experimental set of vapor pressure data, the derived enthalpy of mixing value can differ greatly as shown the first version in [23] and then the revised revision in [18].

The experimental results on enthalpy of formation of the Mg_2Si phase are scattering from -21.1 to -29.7 kJ (mol-atom)$^{-1}$ [26–28], while the *ab initio* calculations shows less negative values in the range of to -15.4 to -18.2 kJ mol-atoms^{-1} [6,12,29]. In this work, we also essentially accept the value near -21 kJ mol-atoms^{-1} which was measured by [26] and used for optimization. The enthalpy of fusion of the Mg_2Si phase was measured as 27.1 ± 2.7 kJ mol-atoms^{-1} in [26] and 19.6 ± 1.5 kJ mol-atoms^{-1} in [12]. Based on the low temperature heat capacity (C_p) measurement, the absolute entropy of Mg_2Si at 298 K ($S^0_{298.15}$) was experimentally determined to be 27.61 J mol^{-1} K^{-1} [30] and 25.27 J mol^{-1} K^{-1} [31], and the *ab initio* calculations [12] are close to the experimental results in [31]. In the present work, the experimental C_p data in [31] are used to optimize the C_p function of the Mg_2Si phase down to 0 K. In order to validate the phase diagram calculations down to 0 K the Gibbs energy functions of the solid phases are also evaluated as described below.

4. Thermodynamic modeling with the new LET function

The Gibbs energy function of the pure element (i) (i=Mg and Si), in any phase ϕ (ϕ=liquid, hcp, diamond) is described by an equation of the following form:

$$G_i^{0,\phi}(T) = A + B{\cdot}T + C{\cdot}T{\cdot}\ln T + D{\cdot}T^2 + E{\cdot}T^3 + F_1{\cdot}T^{-1} + F_2{\cdot}T^4 + F_3{\cdot}T^{-9} \quad (11)$$

Here $G_i^{0,\phi}(T) = G_i^{\phi}(T) - H_i^{SER}$ describes the Gibbs energy function, of the pure element (i) in any phase ϕ, while H_i^{SER} is the molar enthalpy of that element (i) at 298.15 K and 1 bar in its standard element reference (SER) state. The "0" in $G_i^{0,\phi}(T)$ defines the so-called SER-reference state, which is, thus, transferred to all phases in the subsequent equations. The Gibbs energy function of element (i) in its SER phase, ϕ=SER, is often denoted as GHSER$_i$, GHSER$_i$ = $G_i^{0,SER}(T)$. Eq. (11) is capable of describing also the temperature ranges below 298 K as demonstrated in [32] and applied here for the Mg–Si system.

The Gibbs energy functions for Mg-hcp ($G_{Mg}^{0,hcp}$), Si-diamond ($G_{Si}^{0,diamond}$) and Si-hcp ($G_{Si}^{0,hcp}$) above 298 K are taken from the SGTE (V5.1b) database (Scientific Group Thermodata Europe) [33], which is identical to the print version [34]. As no data are available for Mg in diamond structure ($G_{Mg}^{0,diaomnd}$) in the SGTE pure element database, we accept the value of +74780 J mol^{-1} for the enthalpy of formation at 0 K resulting from density functional theory calculations, published in the *Open Quantum Materials Database* (OQMD) created by Chris Wolverton's group at Northwestern University [http://oqmd.org/]. That value was taken as an approximately constant value of the lattice stability, $G_{Mg}^{0,diamond}(T) - G_{Mg}^{0,hcp}(T) = 74780$ J mol^{-1}.

The Gibbs energy of the compound Mg_2Si is described with absolute reference state, thus enabling the quantitative description of the heat capacity:

$$G^{Mg_2Si}(T) = A + B{\cdot}T + C{\cdot}T{\cdot}\ln T + D{\cdot}T^2 + E{\cdot}T^3 + F_1{\cdot}T^{-1} + F_2{\cdot}T^4 \quad (12)$$

The coefficients C, D, E, F_1, F_2 are heat capacity terms and can be determined from the temperature dependence of the heat capacity of Mg_2Si ($C_p^{Mg_2Si}$):

$$C_p^{Mg_2Si}(T) = -C - 2{\cdot}D{\cdot}T - 6{\cdot}E{\cdot}T^2 - 2{\cdot}F_1{\cdot}T^{-2} - 12{\cdot}F_2{\cdot}T^3 \quad (13)$$

The heat capactiy of Mg_2Si phase above 298.15 K is accepted from the previously well assessed equation in [12]. The heat capacity equations below 298.15 K are curve fitted based on the experimental data of [31], which cover the temperature range from 308 K down to 16 K. The curve fittings start from 298.15 to 0 K, and make sure the C_p and the first derivative of C_p (i.e. C_p') are continuous at each temperature breaking points. For the lowest temperature range of 0–17 K, only two terms were used from Eq. (13):

$$C_p^{Mg_2Si}(T) = -2{\cdot}D{\cdot}T - 12{\cdot}F_2{\cdot}T^3 \quad (0 \le T \le 17\ K) \quad (14)$$

The values of the coefficients D and F_2 can be solved by the continuity condition of C_p and C_p' at 17 K. After the C_p equations at all temperature ranges down to 0 K have been determined, the value of coefficient B in each temperature range was determined by the continuity condition of the entropy of Mg_2Si with the constraint of S=0 at 0 K. The value of the coefficient A from Eq. (11) for the temperature range $T > 298.15$ K is optimized based on the critically assessed experimental thermodynamic and phase equilibria data. The coefficient A in other temperature ranges can be determined by the continuity condition of Gibbs energy and enthalpy of the Mg_2Si phase.

The heat capacity of pure Mg in the temperature ranges below 298.15 K was curve fitted based on experimental data of [35,36]. The $G_{Mg}^{0,hcp}$ above 298 K is taken from [34] and found to be valid down to 250 K. Again, C_p, C_p' and S are kept continuous at 250 K, and any other lower temperature breaking points. As the S_{298} value in [34] is not the same as the C_p-fitting in this work, the final S at 0 K is a small positive value of 0.03 J K^{-1} mol-atoms^{-1} to maintain continuity at the break points. The parameters for the pure (Si)-diamond are basically taken from our previous work on the Li–Si system [32], however, a revision was made to improve continuity of C_p, C_p' and S at temperature breaking points.

No special effort was made for the low temperature description of the pure liquid components since data are lacking. However, these two functions, $G_{Mg}^{0,Liquid}$ and $G_{Si}^{0,Liquid}$ are linked to the functions $G_{Mg}^{0,hcp}$ and $G_{Si}^{0,diamond}$, respectively, which are properly described down to 0 K. Therefore, the C_p-functions of pure liquid Mg and Si merge with those of the hcp and diamond solid phases, respectively, with decreasing temperature and approach zero at 0 K. The entropy functions, $S_{Mg}^{0,Liquid}$ and $S_{Si}^{0,Liquid}$ approach positive values at 0 K, corresponding to the metastable entropies of melting, changing only little with temperature. This appears as a reasonable approximation in view of missing data.

Thermodynamic calculations and the parameter optimization are performed using the Pandat software package (www.compute rm.com) with PanOptimizer [37]. All thermodynamic Gibbs energy parameters determined in the present work are given in Table 1.

5. Results and discussion

5.1. Phase diagram

Many thermodynamic descriptions of the Mg–Si binary system have been published [6,12,13,26,38–41]. The most recent four Calphad assessments [6,12,13,42] will be used for comparison. Fig. 3 shows the comparison of the Mg–Si phase diagram calculated in the present work with previous Calphad calculations [6,12,13] and experimental data [12,14,16–19,21]. The calculated phase diagram of [42], which used the further modified quasi-

Table 1
Phase names, models (sublattice formula) and parameters of the present thermodynamic description. Gibbs energy is given in J per mol-formula (of sublattice definition), temperature (T) in Kelvin.

Liquid: (Mg, Si)1	
$L^{0,Liquid}_{Mg,Si} = (-59907.1 + 10.0 \cdot T) \cdot E(T)$	
$L^{1,Liquid}_{Mg,Si} = (-20810.1 + 12.2428 \cdot T) \cdot E(T)$	
$L^{2,Liquid}_{Mg,Si} = (26078.6 - 14.0 \cdot T) \cdot E(T)$	
$E(T) = \exp\left[-\left(\frac{T-500K}{\sqrt{2}\cdot 2000K}\right)^2\right]$	
(Mg)-hcp: (Mg, Si)1	
	$(0 < T < 20)$
	$(20 < T < 50)$
$G^{0,hcp}_{Mg} = -5305.5 + 13.7883\,T - 1.4483\,T\ln(T) - 0.07436\,T^2 + 3775\,T^{-1}$;	$(50 < T < 100)$
$G^{0,hcp}_{Mg} = -7329.0 + 117.0914\,T - 21.6833\,T\ln(T) - 0.00691\,T^2 + 37500\,T^{-1}$;	$(100 < T < 250)$
	$(250 < T < 923)$[a]
$G^{0,hcp}_{Mg} = -14130.185 + 204.716215\,T - 34.3088\,T\ln(T) + 1.038192\,10^{28}\,T^{-9}$	$(923 < T < 3000)$[a]
$G^{0,hcp}_{Si} = 49200 - 20.8\,T + G^{0,diamond}_{Si}(T)$	$(0 < T < 3600)$
$L^{0,hcp}_{Mg,Si} = -5330$	
(Si)-diamond: (Mg,Si)1[b]	
$G^{0,diamond}_{Si} = -3217.986 + 0.0138\,T + 5.306\,10^{-6}\,T^2 - 7.32\,10^{-7}\,T^4$;	$(0 < T < 20)$
	$(20 < T < 100)$
	$(100 < T < 298)$
	$(298 < T < 1687)$
$G^{0,diamond}_{Si} = -9457.642 + 167.281367\,T - 27.196\,T\ln(T) - 4.20369\,10^{30}\,T^{-9}$;	$(1687 < T < 6000)$
$G^{0,diamond}_{Mg} = 74780 + G^{0,hcp}_{Mg}(T)$	$(0 < T < 6000)$
$L^{0,diamond}_{Mg,Si} = 40618.0 - 38\,T$	
Mg_2Si: (Mg)2(Si)1	
$G^{Mg_2Si} = -75335.76 - 0.0052\,T^2 - 1.25\,10^{-7}\,T^4$;	$(0 < T < 17)$
	$(17 < T < 50)$
$G^{Mg_2Si} = -73998.13 - 160.5303\,T + 40.92023\,T\ln(T) - 0.498235\,T^2 + 4.38333\,10^{-4}\,T^3$	$(50 < T < 120)$
$-8007\,T^{-1}$;	
	$(120 < T < 250)$
$G^{Mg_2Si} = -86546.8 + 410.4926\,T - 71.6610\,T\ln(T) - 0.00561\,T^2 + 278010\,T^{-1}$;	$(250 < T < 1400)$[c]
$G^{Mg_2Si} = -96748.07 + 521.8042\,T - 87.0853\,T\ln(T)$;	$(1400 < T < 3000)$

Parameters from other sources:
[a] $G^{0,hcp}_{Mg}$-data from [34] above room temperature are extrapolated down to 250 K;
[b] $G^{0,diamond}_{Si}$-data modified from [32];
[c] Parameters for C_p of Mg_2Si in the range 250 K < T < 1400 K from [12].

chemical model, is not presented here, because our aim is to illustrate the effect of different temperature functions in the substitutional solution model. The invariant reactions in Mg–Si binary system calculated from this work and previous calculations [6,12,13,42] are compared with collected experimental data [12,14–22,43] in Table 2.

Before we proceed to a more detailed comparison of phase diagram and thermodynamic data it is emphasized that the number of adjustable parameters, rising in the previous works from 4 to 6 to 8 [6,12,13] is reduced to 6 in the present work as detailed in Table 3. The occurrence of any artifacts will be discussed at the end of this section.

In the whole composition range, as shown in Fig. 3a, the calculated phase diagram is close to previous calculations [6,12,13] and in good agreement with key experimental data [14,18]. The experimental data of [19,21] are scattering, but they are also in reasonable agreement with the present calculation. It is noted that the liquidus of (Si) appears in better agreement with the experimental data [14] in the range of 70–90 at%Si in the present work.

When we go into more detail in the central part of the phase diagram of Mg–Si system, as shown in Fig. 3b, the congruent melting temperature of this work is 1350.9 K and close to the experimental result of 1351 K in [14] and calculation result in [12]. The calculated congruent melting point of Mg_2Si phase in [6] is 1357.8 K close to the experimental result of 1358 K in [18]. Both [18] and [14] have done dedicated experimental thermal analysis work on the Mg–Si system, and it is difficult to judge which one is superior to the other. It is noted that [14] studied more samples covering the Si-rich eutectic compared to [18]. The Si-rich eutectic liquid composition of 54.1 at% Si was obtained from a separate evaluation by extrapolation of durations at eutectic arrest for constant sample mass of 40 g in [14], which are proportional to the fraction of eutectic heat of solidification. That is superior to the graphical extrapolation of the liquidus temperatures intersecting at 53.0 at% Si for the eutectic liquid in the evaluation of [18]. The data of [14] are also supported by microstructural analysis of the solidified samples. Thus we put some more weight on [14] compared to [18] in this work, as also shown in the comparison of the invariant reactions in Table 2.

The Mg-rich side of Mg–Si phase diagram shown in Fig. 3c compares the present and previous Calphad calculations [6,12,13] with the experimental data [14,16,19,21]. The experimental data from [19,21] are essentially off from the established phase diagram in this region. In the hypoeutectic region of the L=(Mg)+Mg_2Si eutectic reaction, the liquidus temperatures experimentally determined by [14] agree well with the Calphad calculations in this

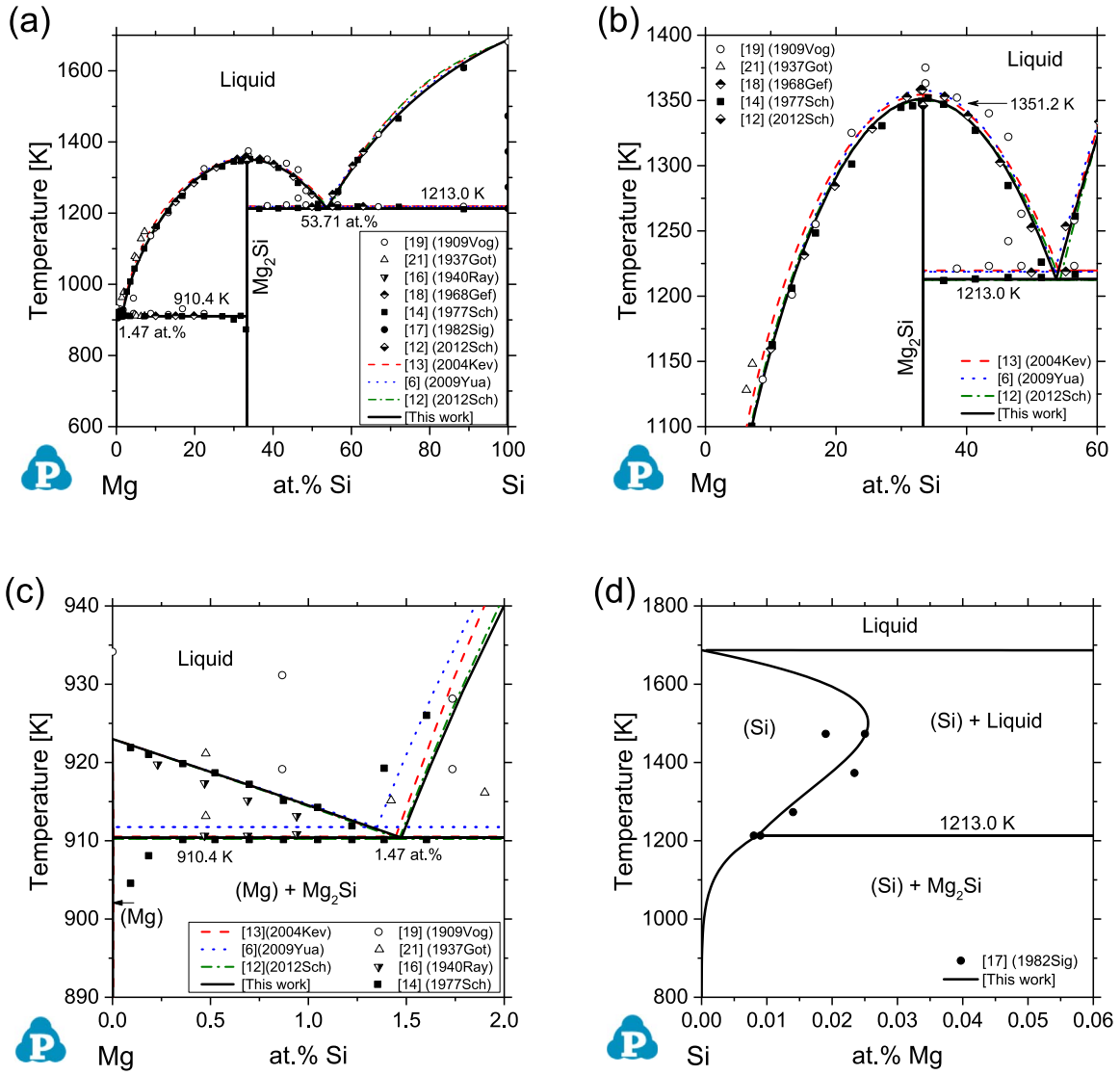

Fig. 3. The calculated Mg–Si phase diagram in the present work compared with the experimental data [12,14,16–19,21], and previous Calphad calculations [6,12,13]. (a) The whole composition range. (b) Enlarged part of Fig. 3a shows the Mg_2Si liquidus in detail. (c) Enlarged part of Fig. 3a shows the Mg-rich eutectic reaction, L=(Mg)+Mg_2Si, in detail. (d) Enlarged part of Fig. 3a shows the solidus and solvus in the Si-rich corner. Additional shorthand-notation for references, indicating year and first author, is provided in brackets.

work and previous publications [6,12,13]. The liquidus lines of (Mg) from all these Calphad calculations essentially overlap, as demanded by thermodynamic laws in this almost dilute region near the melting point of Mg. Therefore, the calculated eutectic temperature is inevitably linked to the calculated eutectic liquid composition. We do accept the experimentally determined eutectic temperature determined consistently at 910.2 K (637 °C) by 14 samples [14]. Only the two Mg-richest samples, indicating a lower temperature, are considered to be impaired by an artifact probably due to the low fraction of eutectic. The interpretation of a significant Si-solubility in (Mg) [14] is not accepted, it is in conflict with the much lower values determined by superior direct experiments [15,16], see Table 2.

The presently calculated eutectic temperature of 910.4 K, thus, fixes the eutectic liquid composition at 1.47 at% Si. The lower value of approx. 1.3 at% Si reported by [14] is considered less relevant since it was obtained by graphical extrapolation of the liquidus temperatures. That was based on the two data points at 1.4 and 1.6 at% Si, showing higher temperatures and interpreted as Mg_2Si liquidus [14]. However, they could relate to a very small thermal signal only because of the small fraction of Mg_2Si and are considered as artifacts here. The higher eutectic temperature of 911.8 K reported by [18] was determined only by three samples with more than 10 at% Si.

The Mg–Si phase diagram in Si-rich corner is shown for the first time in Fig. 3d. The calculated retrograde solidus of (Si) agrees well with the experimental data [17]. A similar level of retrograde solidus of (Si) has also been assessed in the Al–Si binary system [44].

5.2. Thermodynamic data

Table 4 compiles the absolute entropy, enthalpy of formation, and enthalpy of fusion of the Mg_2Si phase obtained by experiments and calculations. The absolute entropy at 298 K in this work is determined by curving fitting of the low temperature heat capacity data in [31]. The slight difference between this work, 25.31 J K^{-1} mol-atoms^{-1}, and the value of 25.27 J K^{-1} mol-atoms^{-1} published in [31] might be due to the different curve fitting adopted in this work and in [31]. The enthalpy of formation calculated in this work is −20.94 kJ mol-atoms^{-1}, close to the experimental data of −21.12 kJ mol-atoms^{-1} in [26]. The enthalpy of fusion of the Mg_2Si phase calculated in this work is 29.3 kJ mol-

Table 2
Calculated invariant reactions in the Mg–Si system compared with experimental and other Calphad-calculated data.

Reaction	Temperature [K]	Composition (at% Si)			Reference, method
		L	(Si)	(Mg)	
L=(Si)+ Mg_2Si	1221/1242[a]	54.4	–	–	[19], exp
	1193	53.4	–	–	[20], exp
	1218.8	53.0	–	–	[18], exp
	1213.2	54.1	–	–	[14], exp
	1219	52.9	–	–	[22], exp
	1215	–	–	–	[12], exp
	1219.7	54.12	100	–	[13], calc
	1218	53.2			[42], calc
	1218.7	53.50	100	–	[6], calc
	1212.5	54.30	100	–	[12], calc
	1213.0	**53.71**	**99.991**	–	**[This work], calc**
L=(Mg)+ Mg_2Si	918.0/931.2[a]	3.48	–	–	[19], exp
	898.2	–	–	–	[20], exp
	–	1.19	–	–	[43], exp
	915.2	1.05	–	–	[21], exp
	910.7	1.16	–	0.003[b]	[16], exp
		–	–	0.0028[c]	[15], exp
	911.8	–	–	–	[18], exp
	910.2	1.30	–	<0.17[d]	[14], exp
	910.5	1.44	–	0.005	[13], calc
	910	1.57			[42], calc
	911.8	1.35	–	0.003	[6], calc
	910.2	1.46	–	0.003	[12], calc
	910.4	**1.47**	–	**0.0028**	**[This work], calc**
L=Mg_2Si	1363/1375[a]	33.7	–	–	[19], exp
	1343	33.7	–	–	[20], exp
	1358	33.1	–	–	[18], exp
	1351	33.3	–	–	[14], exp
	1346	33.33	–	–	[12], exp
	1354.5	33.33	–	–	[13], calc
	1359	33.33			[42], calc
	1357.8	33.33	–	–	[6], calc
	1350.5	33.33	–	–	[12], calc
	1351.2	**33.33**	–	–	**[This work], calc**

[a] The values refer to different purities of Si (92.3% and 99.2%) used in [19]. Experimental methods used for solubility of Si in (Mg) given in footnotes (b) and (d) :
[b] Estimated by X-ray measuring the lattice parameter of (Mg) phase in a Mg-1at%Si sample quenched from 605 °C. [16].
[c] Direct determination in modified zone-melting technique [15].
[d] Approximate value based on two DTA data [14].

atoms^{-1}, within the error bar of the measurement of 27.1 ± 2.7 kJ mol-atoms^{-1} in [26], but much higher than the measured value reported in [12]. It is noted in Table 4 that all calculated enthalpy of fusion values are in the higher range of 28.2 to 31.5 kJ mol-atoms^{-1}. The significantly lower experimental value of 19.6 kJ mol-atoms^{-1} [12] could not be fitted in [12] and the present work.

Fig. 4 represents the calculated activity of Mg in liquid phase at 1350 K compared with the experimental data [18,23–25]. The calculated result in this work is in reasonable agreement with the experimental data of [23]. In [24], both the measured electromotive force (E) values together with the calculated activity values are published. By checking that simple calculation we find that, strangely, there is a significant mismatch. As shown in Fig. 4 the published activity values, denoted as (1964Sry)-1 [24] are significantly lower compared to those recalculated from the published E values in the same work, denoted as (1964Sry)-2 [24]. The recalculation is by the equation

Table 3
Number of adjustable parameters used for the Gibbs energy of liquid phase from [6,12,13] and present work.

Total number	Liquid phase interaction parameter	Reference
4	$L^{0,Liquid}_{Mg,Si} = -70055 + 24.98\,T$ $L^{1,Liquid}_{Mg,Si} = -1300$ $L^{2,Liquid}_{Mg,Si} = 6272$	[13]
6	$L^{0,Liquid}_{Mg,Si} = -71994\,\exp(-3.66767\,10^{-4}\,T)$ $L^{1,Liquid}_{Mg,Si} = -100425.45\,\exp(-2.094\,10^{-3}\,T)$ $L^{2,Liquid}_{Mg,Si} = 136741.72\,\exp(-2.13159\,10^{-3}\,T)$	[6]
8	$L^{0,Liquid}_{Mg,Si} = -65336 + 16.6\,T$ $L^{1,Liquid}_{Mg,Si} = -4097.7 - 0.3\,T$ $L^{2,Liquid}_{Mg,Si} = 9912 - 2.35\,T$ $L^{3,Liquid}_{Mg,Si} = 2915 - 3.22\,T$	[12]
6	$L^{0,Liquid}_{Mg,Si} = (-59907.1 + 10.0\,T)\,E(T)$ $L^{1,Liquid}_{Mg,Si} = (-20810.1 + 12.2428\,T)\,E(T)$ $L^{2,Liquid}_{Mg,Si} = (26078.6 - 14.0\,T)\,E(T)$ $E(T) = \exp\left[-\left(\frac{T-500\mathrm{K}}{\sqrt{2}\cdot 2000\mathrm{K}}\right)^2\right]$	[This work]

Table 4
Thermodynamic data of pure solid Mg_2Si: absolute entropy ($S^0_{298.15}$), standard enthalpy of formation ($\Delta H^0_{298.15}$), and enthalpy of fusion at congruent melting point ($\Delta^{fus}H$); the unit mol refer to 1 mol of atoms).

$S^0_{298.15}$ (J mol^{-1} K^{-1})	$\Delta H^0_{298.15}$ (kJ mol^{-1})	$\Delta^{fus}H$ (kJ mol^{-1})	Method	Reference
–	-25.9 ± 2.1	–	Calorimetry	[27]
–	-29.7 ± 3.8	–	Calorimetry	[28]
–	-21.12[a] ± 2.54 -24.23 ± 3.53	27.1 ± 2.7	Calorimetry	[26]
–	–	19.6 ± 1.5	Calorimetry	[12]
27.61 ± 0.14	–	–	Calorimetry	[30]
25.27	–	–	Calorimetry	[31]
–	-17.7	–	*ab initio* (GGA)[b]	[29]
–	-18.2	–	*ab initio*	[6]
25.5	-16.7	–	*ab initio* (LDA)[c]	[12]
26.4	-15.4	–	*ab initio* (GGA)[b]	[12]
25.37	-21.74	31.0	Calphad	[26]
22.86	-21.57	28.4	Calphad	[13]
25.25	-21.62	28.2	Calphad	[42]
26.39	-20.95	31.3	Calphad	[6]
25.31	-21.05	31.5	Calphad	[12]
25.31	**-20.94**	**29.3**	**Calphad**	**[This work]**

[a] This less exothermic value is recommended by [26].
[b] *ab initio* calculation with generalized gradient approximation (GGA) using the Perdew–Burke–Ernzerhof (PBE) parameterization.
[c] LDA: *ab initio* calculation with local density approximation (LDA).

$$-2 \cdot F \cdot E = R \cdot T \cdot \ln a_{\mathrm{Mg}} \tag{15}$$

with F being the Faraday constant, $F/R = 11.6045$ K/mV, and a_{Mg} the activity of Mg. The reference state of pure liquid Mg is given by the experimental setup in [24], employing a liquid Mg reference electrode. The (1964Sry)-2 data at 1423 K, recalculated from the

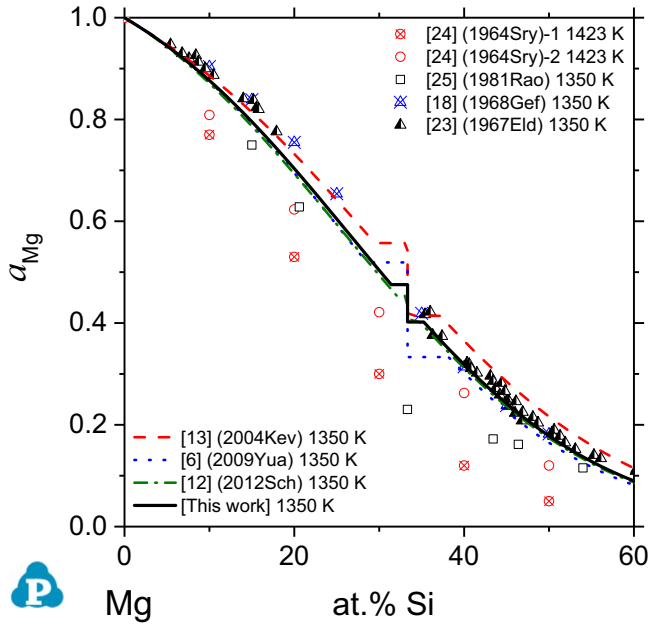

Fig. 4. Calculated activity of Mg in liquid phase, a_{Mg}, at 1350 K (reference state liquid Mg) compared with the experimental data [18,23–25]. (1964Sry)-1: Data from the published activity value in [24]. (1964Sry)-2: Data calculated from the EMF value in [24]. Data in [20] are actually revised calculation data from [23]. The vertical step at 33.33 at% Si is due to the occurrence of solid Mg_2Si.

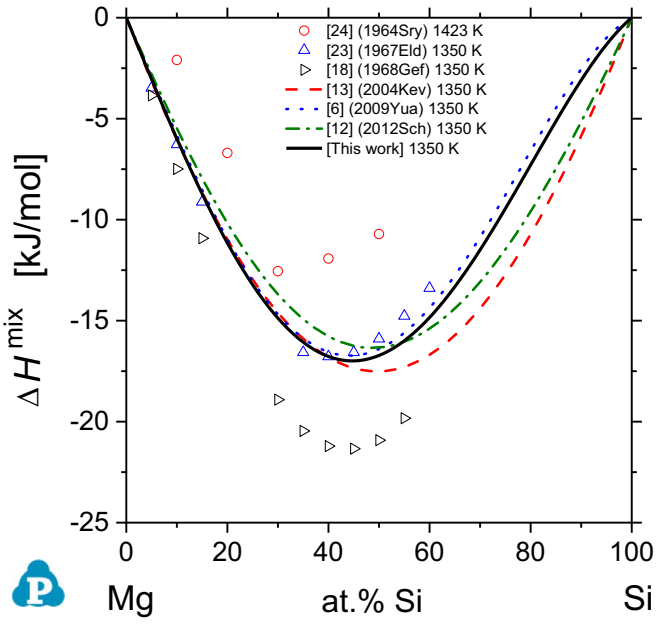

Fig. 5. Calculated enthalpy of mixing in liquid, ΔH^{mix}, at 1350 K compared with derived "experimental" data [18,23,24] and previous Calphad calculations [6,12,13]. Reference states are liquid Mg and liquid Si. Metastable single phase liquid data are shown in the regions where Mg_2Si and (Si) solidify.

original E values [24] are essentially consistent with the data from the EMF measurement at 1350 K reported by [25].

The data of [23] shown in Fig. 4 are the only directly measured activity data, obtained from Mg vapor pressure measurement. Geffken and Miller [18] revised the activity data of [23] by calculation using the phase equilibrium data from their thermal analysis experiments discussed in Section 5.1. These derived activity data are shown in Fig. 4 for comparison only; the revised activity data are close to the direct experimental data from [23].

The enthalpy of mixing in the liquid phase, ΔH^{mix}, is shown in Fig. 5. It is emphasized that none of the "data points" refer to any direct experimental data. They are all derived from some temperature dependence of activity data. The enthalpy of mixing data of [23] reflect the temperature dependence of the original vapor pressure data. The enthalpy of mixing data of [18] reflect the temperature dependence of the revised activity data. It is stunning that such a significant difference can be seen between these two derived enthalpy data sets, [23] and [18], in Fig. 5 even though they stem from the very same original set of experimental vapor pressure data. That is one more example why one should always use direct experimental data in Calphad assessments rather than derived data. The calculated results in this work are coincidently close to the derived data in [23].

Fig. 6 represents the partial enthalpy of mixing of Si in the Mg-rich corner of the liquid phase. The direct experimental data [26] are scattering and do not show a clear trend for compositional dependence. The calculated partial enthalpy curve of the same authors [26], being almost constant at −57 kJ/mol in the composition range of Fig. 6, compares well with the present calculation at 1003 K in that range. In that thermodynamic assessment [26] a total number of 10 (!) L-parameters with linear temperature dependence was used, compared to the 8 parameters in [12], see Table 3.

The temperature dependencies implied in the *LET* function are further explored in Fig. 7 the enthalpy of mixing in the liquid phase. As shown in Fig. 7, the ΔH^{mix} curves at 1350 K and 2000 K are very close to each other and cannot even be distinguished in the Mg-rich side. Even at 700 K, in the supercooled region well below the lowest eutectic at 910 K, the values of ΔH^{mix} do not change dramatically compared to the curve at 2000 K. That is consistent with the intention of the *LET* function, to provide insignificant temperature dependence of ΔH^{mix} in the experimentally accessible region, as often observed experimentally. At very high temperature, however, the ΔH^{mix} effect decreases significantly, as shown at 5000 K, and essentially vanishes at 8000 K. That is consistent with the expectation of essentially ideal interactions on approaching very high temperature. This generally

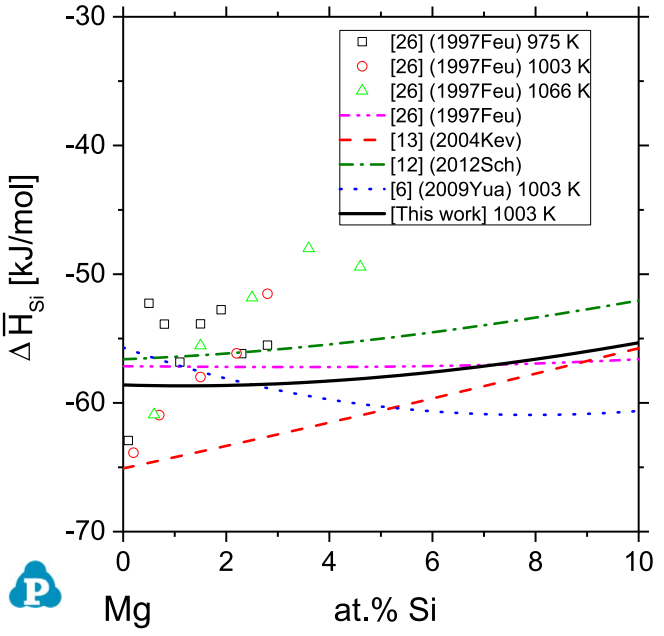

Fig. 6. Calculated partial enthalpy of mixing of Si, $\Delta\overline{H}_{Si}$, in Mg-rich corner of the liquid phase at 1003 K compared with experimental data [26] and previous Calphad calculations [6,12,13,26]. Reference state is liquid Si. The calculated values of [12,13,26] are temperature independent.

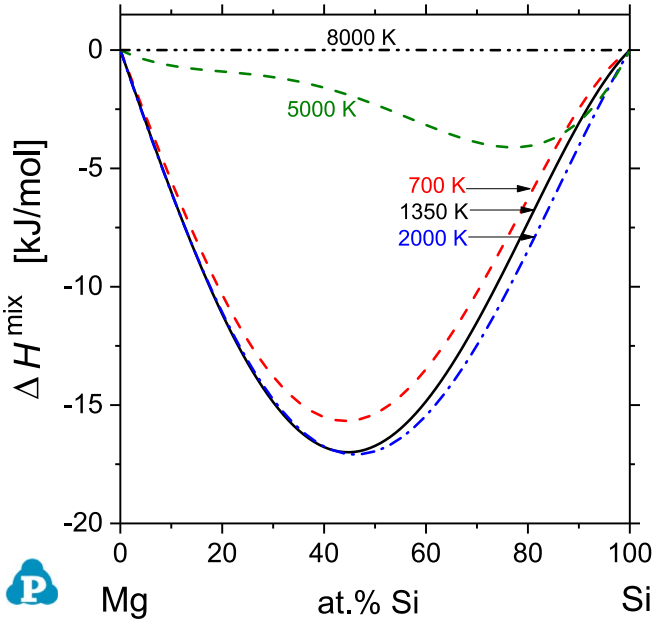

Fig. 7. Calculated enthalpy of mixing in liquid phase, ΔH^{mix}, at various temperatures using the new *LET* function. Reference states are liquid Mg and liquid Si.

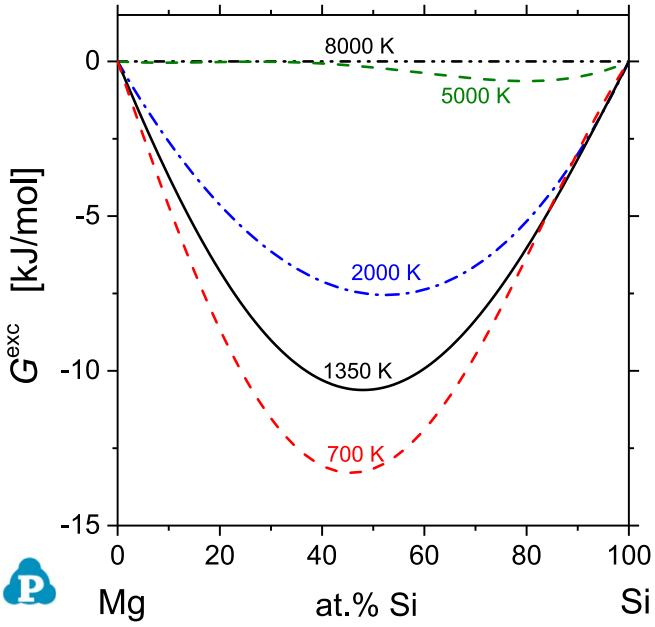

Fig. 8. Calculated excess Gibbs energy in liquid phase, G^{exc}, at various temperatures using the new *LET* function. Reference states are liquid Mg and liquid Si.

realistic tendency is also observed for the excess Gibbs energy of mixing in the liquid, G^{exc}, in Fig. 8. The values of G^{exc} decrease steadily with temperature and eventually fade out, becoming zero at the high-temperature end.

5.3. Thermodynamic excess properties at constant composition of the melt

Figs. 9 and 10 represent the evolution of the thermodynamic excess properties with temperature from 0 to 8000 K in the Mg–Si liquid phase at constant 40 at% Si (60 at% Mg) and 80 at% Si (20 at% Mg), respectively. The two curves for the Mg–Sn melt, shown in red, will be discussed later. Four curves for the different models for Mg–Si are shown in each diagram, labeled as LET: Eqs. (6), (7d) and Table 1 from this work, E: Exponential functions [6], L: Linear functions [12], and Q: Modified quasi-chemical model [45]. Calculations with the modified quasi-chemical model were performed using the software Factsage7.0 [46] and the Factsage database FTLite6.0 [45].

This example for the real Mg–Si system may be compared with the simple hypothetical case of the regular A–B system in Fig. 2. Since at least the sub-sub-regular solution with three *L*-parameters is necessary to describe the Mg–Si melt quantitatively it is more instructive to view their combined impact on $G^{exc}(T)$ at constant composition as opposed to three (or more) graphs of $L(T)$. Following the sequence of the discussion of Fig. 2 let us also discuss Figs. 9 and 10 in the sequence G^{exc}, S^{exc}, ΔH^{mix}, and $C_p{}^{exc}$.

In the temperature range between 900 K and 1700 K, covering the liquidus temperatures of the Mg–Si system, there is no good reason to exclude any of the four descriptions of G^{exc} in Figs. 9 (a) and 10(a). The present calculation using the *LET* functions resembles more closely the usually expected linear behavior with relatively small curvature as opposed to the exponential functions [6]. It is noted that the modified quasi-chemical model, Q, produces almost the same behavior as the linear functions, L, from 900 K to very high temperature. The reason is probably that fairly small short-range order needs to be considered in the modeling of Mg–Si melts (compared to the Mg–Sn melt discussed later). Also, the parameters of the modified quasi-chemical model, the Gibbs energies of pair exchange reactions, are usually made linearly temperature dependent [47]. Only below 900 K and for 60 at% Mg, Fig. 9(a), does the curve Q veer off to very negative values, even more negative than the exponential curve E. That is not generally the case as seen by the almost linear behavior of the curve Q in Fig. 10(a).

By simple extrapolation of the linear functions to much higher temperatures large positive values of $G^{exc}(T)$ are obtained. That results in an inverse liquid miscibility gap above 9150 K with the parameter set of [13]; that curve is omitted in Figs. 9 and 10 for clarity. Extrapolating the parameter set of [12], line L in Figs. 9 and 10, to extremely high temperature of formally 22,440 K the re-stabilization of the Mg_2Si solid phase is calculated, which is just a result of destabilization of the competing liquid phase. At these extremely high temperatures the extrapolated functions for the thermodynamic properties of condensed phases become irrelevant and one might simply ignore any artifacts above 10000 K. However, in multicomponent systems with such a binary edge system the artifact-temperature may be lowered, so care should be taken. In essence, the linear Eq. (2) for *L*-parameters should be avoided if large negative values of the excess entropy, S^{exc}, are obtained as seen by the steep slope of G^{exc} for line L [12] in the examples of Figs. 9 and 10. Both the exponential functions, Eq. (3) [6] and the present *LET* functions, Eqs. (6), (7d) avoid any high-temperature artifacts by construction since G^{exc} must tend to zero for $T \rightarrow \infty$. The *LET* functions, however, approach the expected ideal behavior at $G^{exc} = 0$ more rapidly, as shown in Figs. 9(a) and 10(a).

The more significant distinction between the exponential and the *LET* functions is obvious at the low-temperature end. For the 60Mg40Si (at.%) alloy at 10 K we find values of $G^{exc} = -14.7$ kJ mol^{-1} and $S^{exc} = -1$ J mol^{-1} K^{-1} for the *LET* functions, as opposed to $G^{exc} = -20.6$ kJ mol^{-1} and $S^{exc} = -13.4$ J mol^{-1} K^{-1} for the exponential functions, curves E [6], see Fig. 9(a) and (b). That is the typical exaggeration of the excess quantities implied in the exponential functions, already discussed above in the general features. For the 20Mg80Si alloy at 10 K, Fig. 10(a) and (b), again moderate values are obtained with the *LET* functions, $G^{exc} = -5.9$ kJ mol^{-1} and $S^{exc} = +1$ J mol^{-1} K^{-1}. A peculiar result is obtained for the exponential functions [6] with strongly positive values of $G^{exc} = +5.6$ kJ mol^{-1} and $S^{exc} = +32$ J mol^{-1} K^{-1}. Extremely negative values are calculated in the extrapolation of

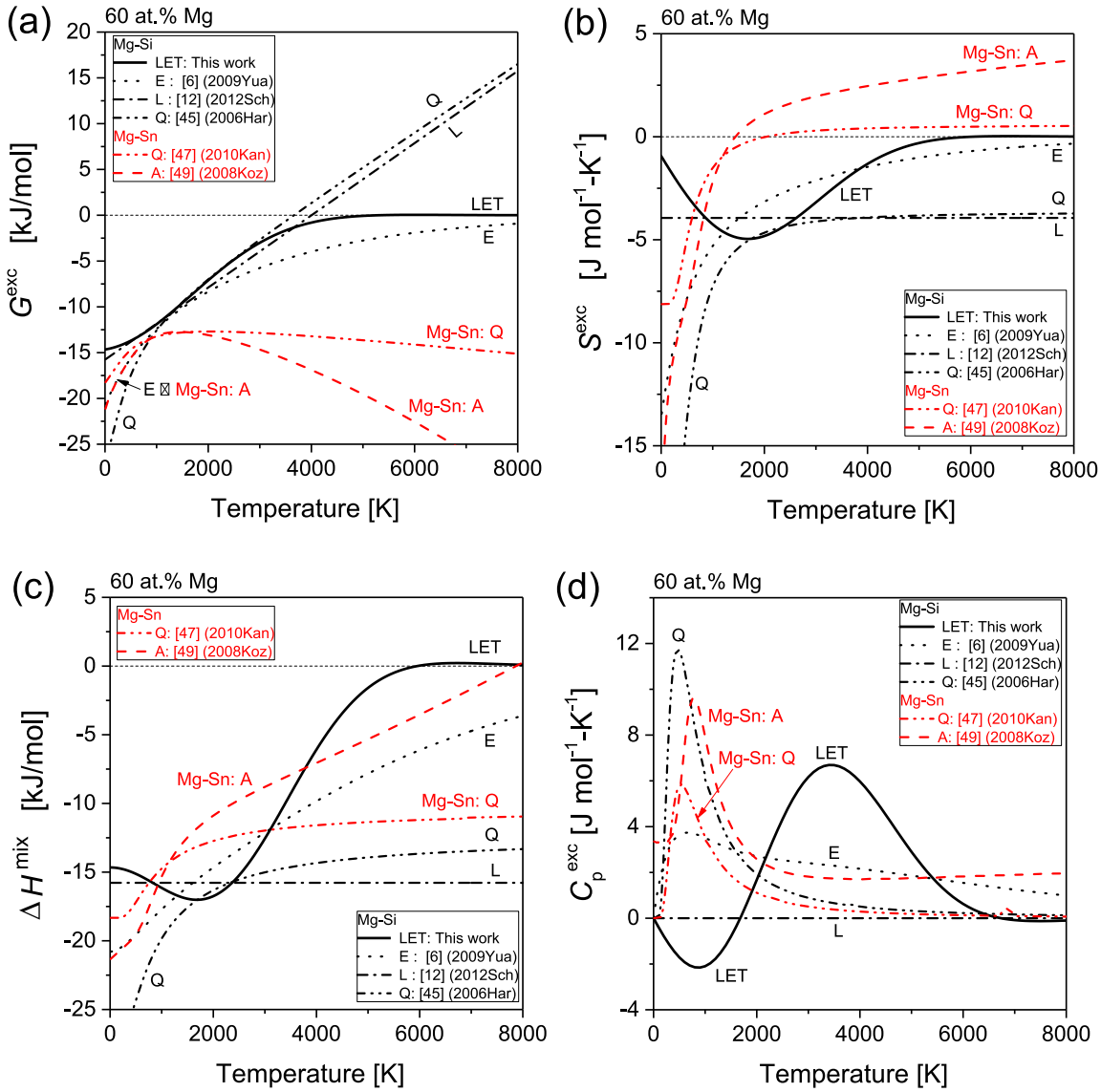

Fig. 9. Excess properties of the liquid phase at constant 60 at% Mg in the Mg–Si system and Mg–Sn system. (a) Excess Gibbs energy; (b) excess entropy; (c) enthalpy of mixing; (d) excess heat capacity. Curve labels are: LET: this work. E: Exponential functions [6]. L: Linear functions [12]. Q: Modified quasi-chemical model [45,47] A: Associate solution model [49]. (For interpretation of the references to color in this figure, the reader is referred to the web version of this article.)

curve Q to 10 K for the 60Mg40Si alloy with $G^{exc} = -27$ kJ mol^{-1} and $S^{exc} = -22$ J mol^{-1} K^{-1}, Fig. 9(a) and (b), compared to the moderate values for the 20Mg80Si alloy, $G^{exc} = -10$ kJ mol^{-1} and $S^{exc} = -3.3$ J mol^{-1} K^{-1}, Fig. 10(a) and (b).

The temperature dependence of the enthalpy of mixing, ΔH^{mix}, for these two Mg–Si alloys is plotted in Figs. 9(c) and 10(c). The general anticipation of fairly small temperature dependence is "best" given by the linear curve L with $\Delta H^{mix} = -15.8$ and -9.6 kJ mol^{-1}, respectively. Between 900 K and 1700 K the values obtained with the *LET* functions vary moderately from -15.9 to -17 kJ mol^{-1}, Fig. 9(c), and from -6.5 to -8.3 kJ mol^{-1}, Fig. 10(c).

The variation given by curve Q is also modest in that range, from -20.5 to -17 kJ mol^{-1}, Fig. 9(c), and even less in Fig. 10(c). The exponential functions, curve E, vary moderately for alloy 60Mg40Si in Fig. 9(c) but show the largest relative variation of all descriptions from -3.4 to -7.8 kJ mol^{-1} in Fig. 10(c). At lower temperature curve E even extrapolates to positive, endothermic behavior below 600 K.

The behavior of the liquid phase description of G^{exc}, resulting in S^{exc} and ΔH^{mix}, at very low temperature may be not so relevant at e.g. 10 K. However, it is very important to use an artifact-free description providing sensible extrapolation for alloys supercooled below their liquidus. That is even more important for applications to multicomponent supercooled liquid alloys, implying both the compositional extrapolation from the Redlich–Kister scheme and the temperature extrapolation from the $L(T)$ function. The moderate behavior demonstrated for the *LET* functions is considered superior to the sudden and rapid changes shown here for the exponential functions in the Mg–Si melt.

At the high-temperature end both the linear and modified quasi-chemical descriptions, curves L and Q in Figs. 9(c) and 10(c), remain at large exothermic values, even at 8000 K, as opposed to the expectation of ideal behavior. Curves E show the expected approach to zero enthalpy but not as clearly as the LET functions which have already attained ideal mixing at 8000 K, considering also the vanishing excess entropy.

The excess heat capacity, C_p^{exc}, of the two Mg–Si alloys shown in Figs. 9(d) and 10(d), is calculated as the first derivative of ΔH^{mix}. In the experimentally accessible range around 1300 K small values of C_p^{exc} are expected, reflected "best" by the linear equation with $C_p^{exc} = 0$. Reasonably small values are obtained in that range with the *LET* functions as seen at the minima of -2.1 and

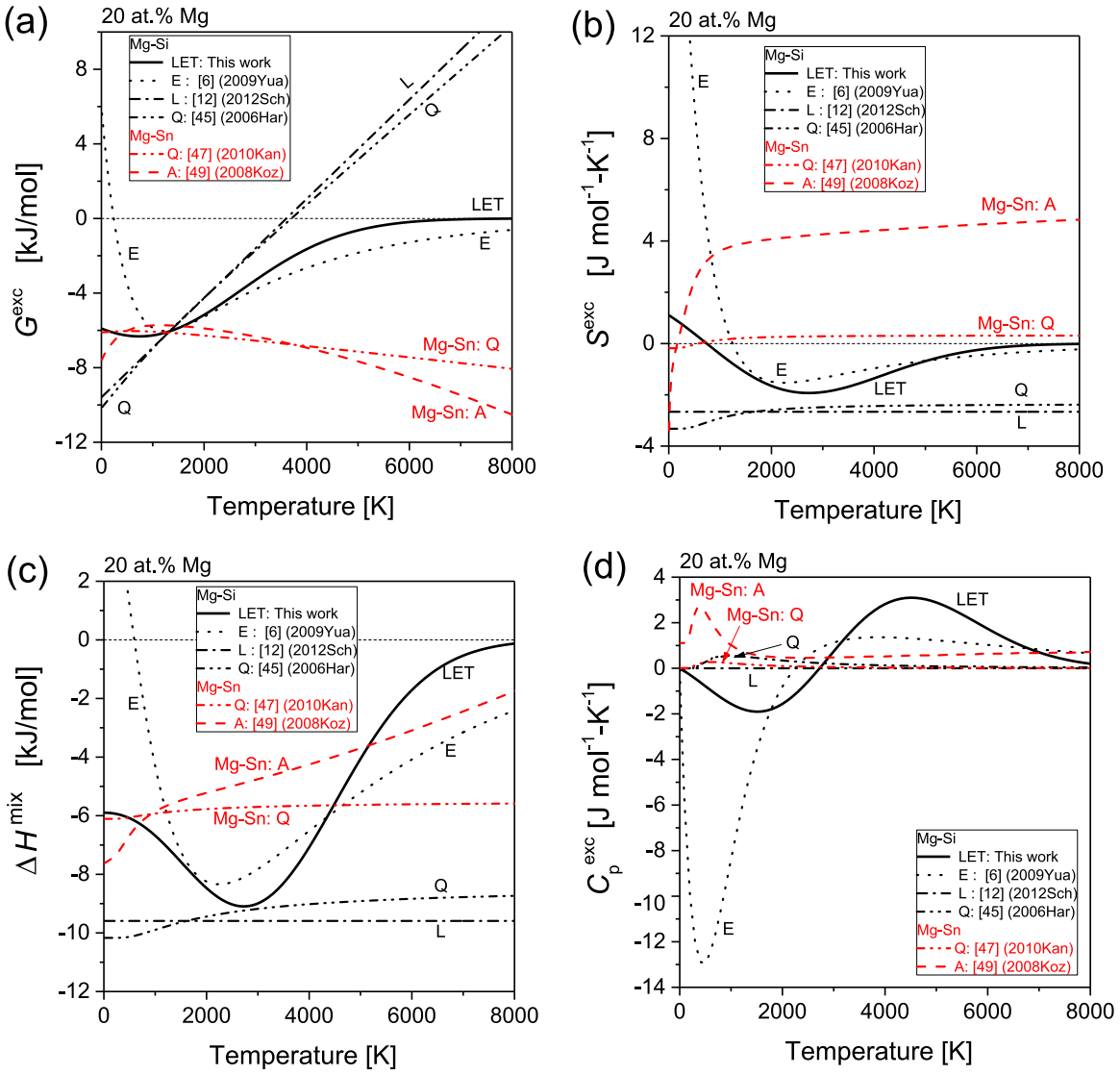

Fig. 10. Excess properties of the liquid phase at constant 20 at% Mg in the Mg–Si system and Mg–Sn system. (a) Excess Gibbs energy; (b) excess entropy; (c) enthalpy of mixing; (d) excess heat capacity. Curve labels are: LET: This work. E: Exponential functions [6]. L: Linear functions [12]. Q: Modified quasi-chemical model [45,47] A: Associate solution model [49]. (For interpretation of the references to color in this figure, the reader is referred to the web version of this article.)

-1.9 J mol^{-1} K^{-1} at 900 K and 1500 K in Figs. 9(d) and 10(d), respectively. The modified quasi-chemical description, curve Q, gives a large value of 7.3 J mol^{-1} K^{-1} at 900 K for alloy 60Mg40Si in Fig. 9 (d) but very small values for alloy 80Mg20Si. Very large values are obtained for the exponential functions, curve E, with -9.6 and 3.6 J mol^{-1} K^{-1} at 900 K in Figs. 9(d) and 10(d), respectively.

The *LET* functions are designed to produce the expected almost constant ΔH^{mix} at lower temperature while approaching zero (ideal behavior) at infinite temperature. Thus, a single high-temperature maximum of C_p^{exc} must necessarily exist, as explained for the hypothetical case in Fig. 2(c) and (d). That unavoidable high-temperature maximum occurs at 3400 K and 4400 K in Figs. 9 (d) and 10 (d), respectively. Beyond that C_p^{exc} also approaches zero as required for ideal behavior.

The two curves for the Mg–Sn melt, shown in red in Figs. 9 and 10, represent an example for a liquid alloy phase with strong short-range order. Two alternative models were used, the modified quasi-chemical model data from Factsage database FTLite [47] and the associate solution model data from Fries and Lukas [48], the corrected parameters are given in [49]. The curves in Figs. 9 and 10 are labeled as Q: modified quasi-chemical model [47], and A: associate solution model [49]. The impact of using these real examples for the two alloys 60Mg40Sn and 20Mg80Sn (at%) on the temperature dependence of G^{exc}, S^{exc}, ΔH^{mix}, and C_p^{exc} is seen by reviewing Figs. 9 and 10. It is also interesting to compare the curves Q for the Mg–Si and Mg–Sn alloys. The associate solution model, curves A, have been applied only for the strong short-range order (Mg–Sn), but not for the case of insignificant short-range order (Mg–Si).

A general feature of the Mg–Sn descriptions of G^{exc} in Figs. 9 (a) and 10(a) is that both curves Q and A do not at all approach ideal behavior at higher temperature. Beyond 1500 K they all tend towards more negative values. That is of course due to the setting of the interaction parameters. For example, the Gibbs energy of formation of the liquid associate Mg_2Sn is represented by an equation in the form $\Delta G^{0,Liquid}(Mg_2Sn) = a + bT + cT\ln(T)$ [48,49], tending to very negative values at high temperature. The Gibbs energy of pair exchange reactions in the Mg–Sn melt in the modified quasi-chemical model [47] are linearly temperature dependent, also tending toward more negative values at high temperature. The aspired trend towards ideal behavior with increasing temperature could be accomplished in both models, A and Q, by using the proposed *LET* function for the interaction parameters. The larger values of S^{exc} of model A compared to model Q are

mainly due to using the negative $cT\ln(T)$ term in model A [48,49].

If we take ΔH^{mix} as an indication of the "bond energy" we can see at least a reasonably continuous trend towards less exothermic values with increasing T in both models, more pronounced in curve A compared to curve Q for the Mg–Sn melt in Figs. 9(c) and 10(c). The derivatives, C_p^{exc}, produce relatively high maximum values of the this quantity in Fig. 9(d) for the 60Mg40Sn alloy around 1000 K. That is probably quite realistic considering the actually measured temperature dependence of ΔH^{mix} between 1073 and 1213 K. The sharp compositional minimum of the experimental data of ΔH^{mix}, shown in [48,49], is located close to the 60Mg40Sn alloy composition, indicating the strong short-range order. That is also reflected by the much smaller values of C_p^{exc} in Fig. 10(d) for the 80Mg20Sn alloy.

5.4. Mg–Si phase and potential diagram from 0 K to high temperature

The capability of the *LET* function is also demonstrated for the calculation of the Mg–Si phase diagram from zero K to high temperature, shown in Fig. 11 for the first time. Instead of silicon composition the chemical potential of Si, μ_{Si}, is used as abscissa. Pure solid Si (diamond structure) is chosen as reference state in this plot:

$$\mu_{Si} - \mu_{Si}^{0,dia} = R{\cdot}T{\cdot}\ln a_{Si} \quad (16)$$

The single phase region of (Si) exhibits negligible extension in this plot and virtually coincides with the vertical axis at $\mu_{Si}-\mu_{Si}^{0,dia}=0$ (or $a_{Si}=1$) up to the melting point of Si at 1687 K. The line of the two-phase region (Mg)+Mg_2Si extends reasonably down to zero Kelvin and any artifact of re-stabilized liquid is avoided by using the *LET* function. The comparison to the previous calculations [6,12,13] is shown only for temperatures above 298 K since these three parameter sets do not include the description of the solid phases down to 0 K.

Another view of the Mg–Si phase diagram is shown in Fig. 12 with the chemical potential of Mg, μ_{Mg}, as abscissa. Here we use pure liquid Mg as reference state:

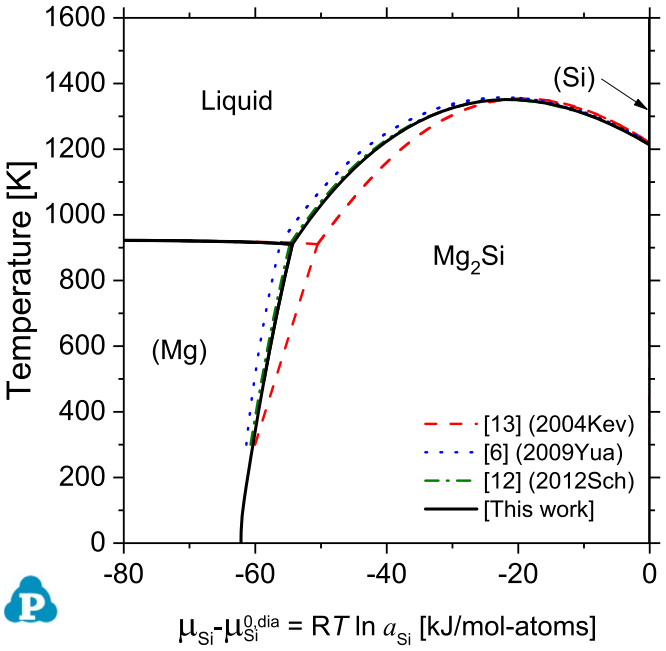

Fig. 11. Calculated Mg–Si phase diagram, using chemical potential of Si as abscissa, from 0 K to high temperature in this work compared to previous calculations above 298 K [6,12,13]. Reference state pure solid Si (diamond).

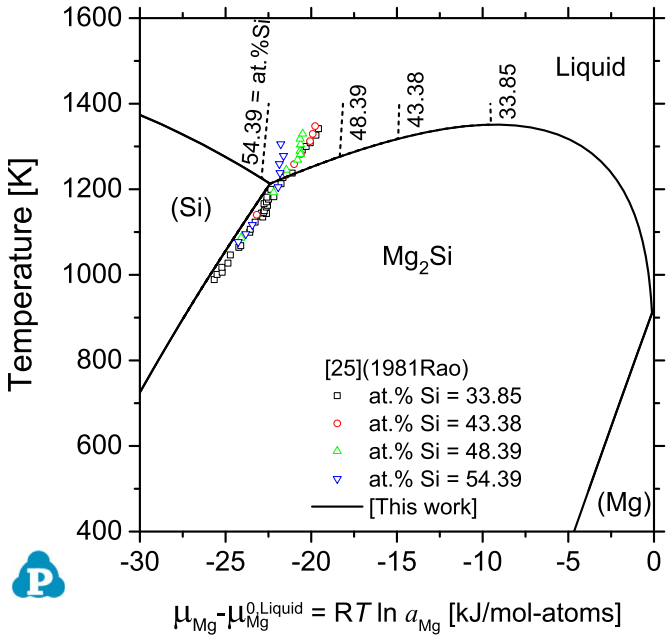

Fig. 12. Calculated Mg–Si phase diagram, using chemical potential of Mg as abscissa. Dashed lines indicate the relation in single phase liquid at four constant alloy compositions. For comparison the experimental data of Ref. [25] are superimposed; most of them were considered [25] to pertain to the (Si)+Mg_2Si and Liquid+Mg_2Si two-phase regions and only few to single phase liquid. Reference state pure liquid Mg.

$$\mu_{Mg} - \mu_{Mg}^{0,liq} = R{\cdot}T{\cdot}\ln a_{Mg} \quad (17)$$

Because of this choice of reference state the single phase region of solid (Mg) appears wider in the bottom right corner. Therefore, the strong bend at the intersection of the two-phase lines (Mg)+Mg_2Si and Liquid+Mg_2Si must occur at the Mg-rich eutectic at 910.4 K. A similar bend occurs at the intersection of the calculated two-phase lines (Si)+Mg_2Si and Liquid+Mg_2Si at the Si-rich eutectic at 1213.0 K.

However, the original experimental EMF data reported by [25] do not show that bend. The EMF was measured with four fixed alloy compositions, given in Fig. 12, between 975 and 1350 K. The reported E values were just recalculated using Eq. (15) and plotted as chemical potential difference of Mg in Fig. 12, given that a liquid Mg reference electrode was used [25], in accord with Eq. (17). All the four alloys are on the Si-rich side of Mg_2Si, the Si-richest contains 54.39 at% Si. Below the eutectic temperature the alloys are in the two-phase region (Si)+Mg_2Si and the experimental data are essentially consistent with the calculated two-phase line, just parallel shifted to higher values of a_{Mg}. Above the eutectic temperature most alloys enter first the two-phase region Liquid+Mg_2Si before some are reaching the fully liquid region. Stunningly, those data points in the Liquid+Mg_2Si region fall on an almost perfect straight line extrapolated from the (Si)+Mg_2Si region, both in the original E *vs.* T plot of [25] in Fig. 12. That is a thermodynamic impossibility as demonstrated by the strong bend in the properly calculated lines in Fig. 12. One can only assume that some artifact in the EMF setup occurred once the equilibrated (Si)+Mg_2Si alloy sample became partly molten.

The calculation also shows the expected temperature *vs.* chemical potential relation of the four alloys upon entering the single phase liquid region by dashed lines in Fig. 12. The corresponding experimental data points show at least qualitatively the same behavior by veering off almost vertically from the two-phase baseline, as seen best for the alloy with 54.39 at% Si. Quantitative

agreement cannot be expected because of the inacceptable experimental Liquid+Mg_2Si base line. The disagreement of the experimental results of [25] in the single phase liquid region with other experimental data at 1350 K was also shown in Fig. 4.

The experimental data of [25] in Fig. 12 have not been shown or discussed in any of the previous Calphad assessments of the Mg–Si system. They have not been used for the present parameter optimization but only shown for comparison. It is noted that all of the experimental data in the equilibrated solid state alloys, (Si)+Mg_2Si, could be perfectly fitted by changing just the first parameter of G^{Mg_2Si} from (–86546.8+….) to (−85650+…). That makes Mg_2Si less stable and produces the parallel shift of the calculated (Si) + Mg_2Si two-phase line to the right hand side in Fig. 12 to match with the experimental data. This constant ΔG of 897 J/mol-formula, or 0.3 kJ/mol-atoms, leaves the entropy of formation of Mg_2Si constant but changes the enthalpy of formation from our accepted value, $\Delta H^0_{298.15} = -20.94$ kJ/mol-atoms to the less exothermic value of −20.64 kJ/mol-atoms. It is obvious from Table 4 that such a small change is within the scatter of the experimental data. Thus, the experimental data of [25] in the solid state alloys, (Si) + Mg_2Si, are considered to be in good agreement with the present calculation.

6. Conclusion

The proposed *LET* function for interaction parameters combines several advantages.

(i) It stays close to a linear relation in a wide temperature range, usually accessible to experimental data;
(ii) it avoids excessive values of the interaction parameter by approaching zero for very high temperatures;
(iii) it also avoids excessive values at very low temperatures;
(iv) it uses only two adjustable parameters, same as the classical linear relation;
(v) it is a relatively simple analytical function providing all of these features by design and, thus, it is inherently consistent, no matter what values are chosen for the adjustable parameters a and b in Eq. (6).

The two latter features are the main distinction to Eq. (4) proposed by Kaptay [7]. This equation employs three instead of two adjustable parameters. Moreover, imposing constraints among the three parameters (h, s, τ) may be required to exclude any low temperature artifact as noted in [7]. As opposed to that, the new *LET* function is designed for the unconstrained application of any optimization software, such as PanOptimizer or PARROT; artifacts will be automatically avoided.

It is suggested to apply the *LET* function only if necessary. For many alloy systems the classical linear relation is sufficient. If, however, artifacts occur during the optimization procedure one should switch to using the *LET* function, Eqs. (6), (7d), instead of the simple linear function. The values a and b obtained at that stage in Eq. (2) might be used as initial values for Eq. (6) in the subsequent final optimization procedure.

The validation of these features and theoretical advantages of the *LET* function was performed by a comprehensive Calphad reassessment of the Mg–Si system. It is demonstrated that the present intrinsically artifact-free description is obtained with a smaller number of adjustable parameters and at least the same good agreement with experimental data as compared to the latest Calphad description [12]. Moreover, for the first time the calculated Mg–Si phase diagram from 0 K to very high temperature is presented. The new assessment also includes the quantitative solidus data of (Si) and other previously not considered original experimental data.

Acknowledgment

This study is supported by the German Research Foundation (DFG) in the Bundled Proposal “PAK461” under Grant no. Schm 588/35.

Appendix

The Gibbs energy for the liquid solution phase is described by the new *LET* function in Eqs. (6), (7d). To make this function compile in software packages Pandat (version 8.2, 2014 and higher) [37] and Thermocalc (version S) [50], the new *LET* function from Eq. (6)(b) may be expanded to the following terms:

$$E(T) = \exp\left[-\left(\frac{T-500\mathrm{K}}{\sqrt{2}\cdot 2000\mathrm{K}}\right)^2\right] = \exp\left[-1.25\times10^{-7}\cdot(T-500)^2\right]$$
$$= \exp(-1.25\times10^{-7}\cdot T^2)\cdot\exp(+1.25\times10^{-7}\cdot 1000\cdot T)$$
$$\cdot\exp(-1.25\times10^{-7}\cdot 250000) = EXP1\cdot EXP2\cdot 0.96923 \quad \text{(A1)}$$

Here we let EXP1 = $\exp(-1.25\times10^{-7}\cdot T^2)$ and EXP2 = $\exp(+1.25\times10^{-7}\cdot 1000\cdot T)$.

In the following lines, the accepted notation of the *LET* function for both Pandat and Thermocalc is shown:

```
---------------------------------------------------------------------------------------
$           LET            = (a+b*T)*E(T)
$ Function FET             =          E(T)
$ T1=500 T2=2000
$ -1.25E-07 = -1/(SQRT(2)*T2)**2
 FUNCTION EXP1   298   EXP(-1.25E-07*T**2); 6000   N !
 FUNCTION EXP2   298   EXP(1.25E-04*T);     6000   N !
 FUNCTION FET    298   +0.96923*EXP1*EXP2;  6000   N !
                                                     .
PARAMETER G(LIQUID,MG,SI;0) 298
-59907.1*FET + 10.0*T*FET; 6000 N !
```

Pandat also accepts the simplified notation:

```
---------------------------------------------------------------------------------------
PARAMETER G(LIQUID,MG,SI;0) 298
 (-59907.1+10.0*T)*FET ; 6000 N !
---------------------------------------------------------------------------------------
```

Appendix A. Supplementary material

Supplementary data associated with this article can be found in the online version at http://dx.doi.org/10.1016/j.calphad.2016.06.003.

References

[1] O. Redlich, A.T. Kister, Algebraic representation of thermodynamic properties and the classification of solutions, Ind. Eng. Chem. 40 (1948) 345–348.
[2] S.L. Chen, S. Daniel, F. Zhang, Y.A. Chang, W.A. Oates, R. Schmid-Fetzer, On the calculation of multicomponent stable phase diagrams, J. Phase Equilib. 22 (2001) 373–378.

[3] G. Kaptay, A new equation for the temperature dependence of the excess Gibbs energy of solution phases, Calphad 28 (2004) 115–124.
[4] H.L. Lukas, S.G. Fries, B. Sundman, Computational Thermodynamics – The Calphad Method, Cambridge University Press, Cambridge, 2007.
[5] R. Schmid-Fetzer, D. Andersson, P.Y. Chevalier, L. Eleno, O. Fabrichnaya, U. R. Kattner, B. Sundman, C. Wang, A. Watson, L. Zabdyr, M. Zinkevich, Assessment techniques, database design and software facilities for thermodynamics and diffusion, Calphad 31 (2007) 38–52.
[6] X. Yuan, W. Sun, Y. Du, D. Zhao, H. Yang, Thermodynamic modeling of the Mg–Si system with the Kaptay equation for the excess Gibbs energy of the liquid phase, Calphad 33 (2009) 673–678.
[7] G. Kaptay, On the abilities and limitations of the linear, exponential and combined models to describe the temperature dependence of the excess Gibbs energy of solutions, Calphad 44 (2014) 81–94.
[8] C.H.P. Lupis, J.F. Elliott, Correlation between excess entropy and enthalpy functions, Trans. Met. Soc. AIME 236 (1966) 130.
[9] G. Kaptay, On the tendency of solutions to tend toward ideal solutions at high temperatures, Metall. Mater. Trans. A 43 (2012) 531–543.
[10] A.A. Nayeb-Hashemi, J.B. Clark, Mg-Si, in: A.A. Nayeb-Hashemi, J.B. Clark (Eds.), Phase Diagrams of Binary Magnesium Alloys, ASM International, Metals Park, Ohio, 1988.
[11] A.A. Nayeb-Hashemi, J.B. Clark, The Mg – Si (magnesium–silicon) system, J. Phase Equilib. 5 (1984) 584–592.
[12] M. Schick, B. Hallstedt, A. Glensk, B. Grabowski, T. Hickel, M. Hampl, J. Gröbner, J. Neugebauer, R. Schmid-Fetzer, Combined ab initio, experimental, and CALPHAD approach for an improved thermodynamic evaluation of the Mg–Si system, Calphad 37 (2012) 77–86.
[13] D. Kevorkov, R. Schmid-Fetzer, F. Zhang, Phase equilibria and thermodynamics of the Mg–Si–Li system and remodeling of the Mg–Si system, J. Phase Equilib. Diffus. 25 (2004) 140–151.
[14] E. Schürmann, A. Fischer, Schmelzgleichgewichte im Dreistoffsystem Aluminium-Magnesium-Silicium Teil 2: Zweistoffsystem Magnesium–Silicium, Giessereiforschung 29 (1977) 111–113.
[15] A.S. Yue, Determination of maximum terminal solid solubility, Trans. Met. Soc. AIME 215 (1959) 870–871.
[16] G.V. Raynor, The constitution of the magnesium-rich alloys in the systems magnesium–lead, magnesium–tin, magnesium–germanium and magnesium–silicon, J. Inst. Met. 66 (1940) 403–426.
[17] H. Sigmund, Solubilities of magnesium and calcium in silicon, J. Electrochem. Soc. 129 (1982) 2809–2812.
[18] R. Geffken, E. Miller, Phase diagrams and thermodynamic properties of the Mg–Si and Mg–Ge systems, Trans. Met. Soc. AIME 242 (1968) 2323–2328.
[19] R. Vogel, Metallographische Mitteilungen aus dem Institut für physikalische Chemie der Universität Göttingen. LXX. Über Magnesium–Siliciumlegierungen, Z. Anorg. Chem. 61 (1909) 46–53.
[20] L. Wöhler, O. Schliephake, Die silicide des calciums und magnesiums, Z. Anorg. Allg. Chem. 151 (1926) 1–20.
[21] M. Goto, M. Nito, H. Asada, Magnesium sheet and alloys, Rept. Aeronautic Research Inst. Tokyo Imp. Univ., 12 (1937) 163-318.
[22] D. Farkas, C.E. Birchenall, New eutectic alloys and their heats of transformation, Metall. Trans. A 16 (1985) 323–328.
[23] J. Eldridge, E. Miller, K. Komarek, Thermodynamic properties of liquid magnesium–silicon alloys. Discussion of the Mg-Group IVB Systems, Trans. Met. Soc. AIME. 239 (1967) 775–781.
[24] I.T. Sryvalin, O.A. Esin, B.M. Lepinskikh, Thermodynamic properties of solutions of magnesium in nickel, lead, and silicon, Russ. J. Phys. Chem. 38 (1964) 637–641.
[25] Y.K. Rao, G.R. Belton, Thermodynamic properties of Mg–Si system, in: N.A. Gokcen (Ed.) Chemical Metallurgy- A Tribute to Carl Wagner, the Metallurgical Society of AIME1981, pp. 75–96.
[26] H. Feufel, T. Gödecke, H.L. Lukas, F. Sommer, Investigation of the Al–Mg–Si system by experiments and thermodynamic calculations, J. Alloy. Compd. 247 (1997) 31–42.
[27] O. Kubaschewski, H. Villa, Bildungswärmen Zintl'scher Erdalkaliverbindungen. Zur Thermochemie der Legierungen XIII, Z. Elektrochem. Angew. Phys. Chem. 53 (1949) 32–40.
[28] R. Blachnik, D. Kunze, A. Schneider, Über eine verbesserte direktkalorimetrische Methode: Bildungsenthalpien der Phasen Mg_2Si und Mg_2Ge, Metall 25 (1971) 119–121.
[29] H. Zhang, S. Shang, J.E. Saal, A. Saengdeejing, Y. Wang, L.-Q. Chen, Z.-K. Liu, Enthalpies of formation of magnesium compounds from first-principles calculations, Intermetallics 17 (2009) 878–885.
[30] W. Mannchen, G. Jacobi, Notizen: Die Molwärme des Mg_2Si von 12° bis 300°K, Z. Naturforsch. B 20 (1965) 178–179.
[31] B.C. Gerstein, F.J. Jelinek, M. Habenschuss, W.D. Shickell, J.R. Mullaly, P. L. Chung, Thermal study of groups II–IV semiconductors. Lattice heat capacities and free energies of formation. Heat capacity of Mg_2Si from 15 – 300 °K, J. Chem. Phys. 47 (1967) 2109–2115.
[32] P. Wang, A. Kozlov, D. Thomas, F. Mertens, R. Schmid-Fetzer, Thermodynamic analysis of the Li–Si phase equilibria from 0 K to liquidus temperatures, Intermetallics 42 (2013) 137–145.
[33] Scientific Group Thermodata Europe Version 5.1b of Unary database - 29 November 2010.
[34] A.T. Dinsdale, SGTE data for pure elements, Calphad 15 (1991) 317–425.
[35] R.S. Craig, C.A. Krier, L.W. Coffer, E.A. Bates, W.E. Wallace, Magnesium–cadmium alloys. VI. Heat capacities between 12 and 320 °K. and the entropies at 25° of magnesium and cadmium, J. Am. Chem. Soc. 76 (1954) 238–240.
[36] P.L. Smith, LXXXIV. The specific heats of magnesium and zinc, London, Edinburgh Dublin, Philos. Mag. J. Sci. 46 (1955) 744–750.
[37] W. Cao, S.L. Chen, F. Zhang, K. Wu, Y. Yang, Y.A. Chang, R. Schmid-Fetzer, W. A. Oates, PANDAT software with PanEngine, PanOptimizer and PanPrecipitation for multi-component phase diagram calculation and materials property simulation, Calphad 33 (2009) 328–342.
[38] P. Dörner, H. Krieg, H.L. Lukas, R. Müller, G. Petzow, The system Mg–Si optimized by a least squares method, Calphad 5 (1981) 41–54.
[39] D. Lüdecke, Phase-diagram and thermochemistry of the Al–Mg–Si system, Z. Met. 77 (1986) 278–283.
[40] N. Chakraborti, H.L. Lukas, Thermodynamic optimization of the Mg–Al–Si phase diagram, Calphad 16 (1992) 79–86.
[41] X.-Y. Yan, Y. Chang, F. Zhang, A thermodynamic analysis of the Mg–Si system, J. Phase Equilib. Diffus. 21 (2000) 379–384.
[42] I.-H. Jung, D.-H. Kang, W.-J. Park, N.J. Kim, S. Ahn, Thermodynamic modeling of the Mg–Si–Sn system, Calphad 31 (2007) 192–200.
[43] W. Schmidt, Beitrag zur Kenntnis der hochprozentigen Magnesiumlegierungen, Z. Met. 10 (1927) 452–455.
[44] S.-M. Liang, R. Schmid-Fetzer, Phosphorus in Al–Si cast alloys: Thermodynamic prediction of the AlP and eutectic (Si) solidification sequence validated by microstructure and nucleation undercooling data, Acta Mater. 72 (2014) 41–56.
[45] Database FTLite (⟨http://www.crct.polymtl.ca/fact/documentation/⟩), with Mg–Si system from J.-P. Harvey, M.A.Sc. thesis, Ecole Polytechnique, Canada, 2006 (VLAB Project); Vol. Data F. Gemme, CRCT, 2003 (VLAB project).
[46] C.W. Bale, E. Bélisle, P. Chartrand, S.A. Decterov, G. Eriksson, K. Hack, I.H. Jung, Y.B. Kang, J. Melançon, A.D. Pelton, C. Robelin, S. Petersen, FactSage thermochemical software and databases — recent developments, Calphad 33 (2009) 295–311.
[47] Database FTLite (⟨http://www.crct.polymtl.ca/fact/documentation/⟩), with Mg–Sn system from: Y.-B. Kang and A.D. Pelton, CALPHAD 34, 2010, pp. 180–188.
[48] S.G. Fries, H.L. Lukas, Optimisation of the Mg–Sn system, J. Chim. Phys. 90 (1993) 181–187.
[49] A. Kozlov, M. Ohno, R. Arroyave, Z.K. Liu, R. Schmid-Fetzer, Phase equilibria, thermodynamics and solidification microstructures of Mg–Sn–Ca alloys, Part 1: Experimental investigation and thermodynamic modeling of the ternary Mg–Sn–Ca system, Intermetallics 16 (2008) 299–315.
[50] J.O. Andersson, T. Helander, L. Hoglund, P. Shi, B. Sundman, Thermo-Calc & DICTRA, computational tools for materials science, Calphad 26 (2002) 273–312.